

Morphological and topological analysis of coarsened nanoporous gold by x-ray nanotomography

Yu-chen Karen Chen,^{1,2,a)} Yong S. Chu,³ JaeMock Yi,² Ian McNulty,² Qun Shen,³ Peter W. Voorhees,¹ and David C. Dunand¹

¹Department of Materials Science and Engineering, Northwestern University, Evanston, Illinois 60208, USA

²Advanced Photon Source, Argonne National Laboratory, Argonne, Illinois 60439, USA

³National Synchrotron Light Source II, Brookhaven National Laboratory, Upton, New York 11973, USA

(Received 26 October 2009; accepted 11 December 2009; published online 29 January 2010)

We used x-ray nanotomography to characterize the three-dimensional (3D) morphology and topology of dealloyed nanoporous gold after coarsening. The interface shape distribution obtained from the nanotomography measurement shows that the coarsening does not proceed by bulk diffusion. The surface normal distribution shows that the morphology of the nanoporous gold is anisotropic. The topology of nanoporous gold is similar to that of other bicontinuous structures created by phase separation, despite the radically different method used to produce the structures. This work opens the door to time-resolved, *in situ* studies of coarsening of nanoporous gold in 3D. © 2010 American Institute of Physics. [doi:10.1063/1.3285175]

Nanoporous gold has numerous potential applications¹ in optical-active materials, catalysts, sensors, mechanical actuators, fuel cell and microbalance electrodes, and as a coating for medical devices. Nanoporous gold is fabricated by dealloying silver-gold solid solutions. This results in fully open-porosity bicontinuous nanoporous structures, following the rearrangement of the gold atoms into interconnected ligaments as the silver atoms are selectively removed.² Optimization of the optical, chemical, and mechanical properties of nanoporous gold depends on its pore size, which is tunable by structural coarsening during annealing.³ Various electron-based techniques have been employed to determine the morphology of nanoporous gold films after dealloying, but none are suited to three-dimensional (3D) study of thick specimens of coarsened nanoporous gold. Tomographic transmission electron microscopy provides very high spatial resolution but is limited to examining thin films, and cannot image coarsened structures once the gold ligament size is close to the electron penetration depth.^{4,5} Focused ion beam (FIB)-scanning electron microscopy serial sectioning⁶ combines high resolution with depth penetration, however, being a destructive method, it cannot be used to observe dynamic processes and structural evolution in 3D. X-ray microcomputed tomography is a powerful nondestructive tomographic tool whose resolution is however typically limited to the micron scale.⁷ Transmission x-ray microscopy (TXM) using synchrotron x-ray sources offers 30 nm resolution, fast image acquisition, and the ability to nondestructively image samples tens of microns thick. Combining TXM with tomographic methods allows complex nanostructures to be imaged in 3D.⁸ Here, we perform x-ray nanotomography on a dealloyed and coarsened nanoporous gold wire. We quantitatively analyze the morphological and topological properties of nanoporous gold from the reconstructed images using methods developed in earlier work.⁹

An Ag-30 at. % Au alloy wire with a diameter of $\sim 50 \mu\text{m}$ was created by drawing the melted alloy within a Pyrex glass tube. When examined by Laue diffraction, the

wire appeared monocrystalline across its diameter and along its $200 \mu\text{m}$ length. The wire protruding from a fracture point of the tube was dealloyed into nanoporous gold by immersion in a nitric acid (75 vol % of commercial nitric acid, 68%–70% assay, in de-ionized water) solution at ambient temperature for 20 h. FIB milling was used to shape a cylindrical tip with $\sim 10 \mu\text{m}$ diameter and $\sim 20 \mu\text{m}$ height. The nanoporous specimen was then coarsened by annealing in air at 400°C for 30 min.

The x-ray nanotomography measurements were carried out using the TXM at beamline 32-ID at the Advanced Photon Source at Argonne National Laboratory. An x-ray energy of 10.4 keV provided excellent Zernike contrast¹⁰ for this $\sim 10 \mu\text{m}$ diameter nanoporous gold specimen. A series of two-dimensional (2D) projection images was collected over a 180° angular range with a 0.5° increment with an exposure time of 1 s per image. The 2D projections were reconstructed in 3D using a filtered-back-projection algorithm.¹¹ Figure 1(a) is a TXM image of the $10\text{-}\mu\text{m}$ diameter nanoporous gold sample. It shows clear contrast between gold (dark) and air. A segmented volume of a smaller $4 \times 3 \times 2 \mu\text{m}^3$ volume [Fig. 1(b)] extracted from the central region of the nanoporous tip clearly shows the internal pore network. This segmented volume was also used to analyze the morphology and topology of nanoporous gold. To quantitatively analyze the

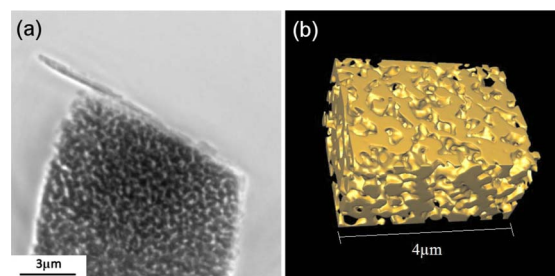


FIG. 1. (Color online) (a) 2D x-ray micrograph showing a projection of the tip of the $\sim 10 \mu\text{m}$ diameter nanoporous gold wire, illustrating the large imaging volume. (b) A small $2 \times 3 \times 4 \mu\text{m}^3$ volume was extracted from the 3D reconstruction of the central region of the tip and segmented for morphological and topological analysis.

^{a)}Electronic mail: yuchenchen2010@u.northwestern.edu.

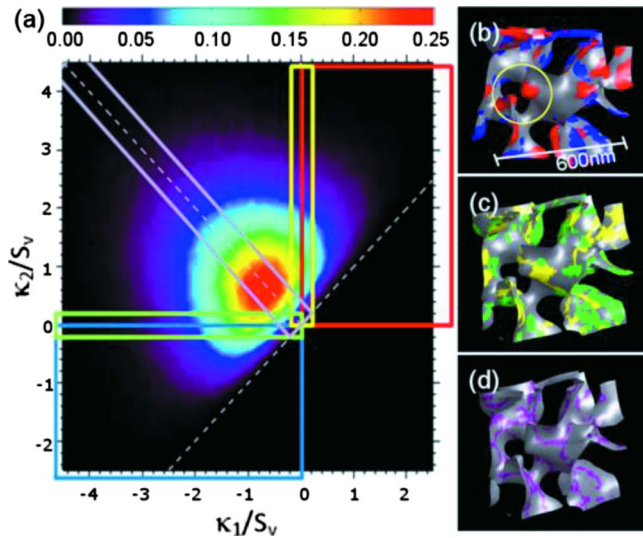


FIG. 2. (Color online) (a) Interfacial shape distribution of nanoporous gold with regions corresponding to particular curvatures are shown in (b), (c), and (d). (b) Convex (red online) and concave (blue online) regions; the circle indicates fission pinch-off of a ligament into two knobs, likely due to coarsening. (c) Transition regions with cylindrical curvature (yellow and green online). (d) Regions with zero mean curvature (purple online).

structure, a surface mesh was generated, from which the surface area per volume, S_v , was found to be 0.00689 nm^{-1} . The inverse value, $S_v^{-1} = 145 \text{ nm}$, corresponds to the characteristic length scale of the structure. Within the entire sample volume, the gold volume fraction was $50 \pm 5\%$, as determined from reconstructed volumes.

We quantified the morphology of the nanoporous gold using the interfacial shape distribution (ISD) method (Fig. 2).¹² The ISD gives the probability of finding a small patch of interface with a given pair of minimum and maximum principal curvatures, κ_1 and κ_2 , respectively. These principal curvatures give the mean curvature, $H = (\kappa_1 + \kappa_2)/2$, which sets the chemical potential at a point on the interface, and the Gaussian curvature, $K = \kappa_1 \kappa_2$. If both κ_1 and κ_2 have the same sign, $K > 0$ and the interfacial patch is parabolic. If their signs are opposite, $K < 0$ and the patch is elliptical or saddle-shaped. In Fig. 2(a), the curvatures are normalized by S_v^{-1} to allow for direct comparison with other bicontinuous structures.

The ISD shape depends on the volume fraction of the phases and the mechanism of mass transport in the system.¹³ As the solid volume fraction departs from 50%, the average of mean curvature deviates from zero. The ISD shown in Fig. 2(a) is symmetric about the zero mean curvature line (dotted line in Fig. 2, where $\kappa_2 = -\kappa_1$). This is consistent with the near zero average mean curvature measured by Fujita *et al.*⁵ for nanoporous gold sample with gold volume fraction similar to ours ($\sim 50\%$) but unlike the positive average mean curvature reported by Rosner *et al.*⁴ for nanoporous gold with lower metal volume fraction (24%). The shape of the ISD for a bicontinuous structure undergoing coarsening by a bulk diffusion mechanism, such as that found during spinodal decomposition,¹⁴ is much different than that shown in Fig. 2(a). Bulk diffusion results in a much smaller range of curvatures in the structure due to the inherent smoothing from diffusion that is driven by bulk concentration gradients. While an evaporation/condensation mechanism yields a qualitatively similar ISD¹⁴ to the present ISD of Fig. 2(a),

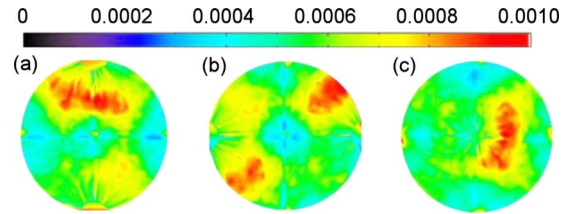


FIG. 3. (Color online) Surface Normal Distributions for nanoporous gold for projections along (a) the x -axis, (b) the y -axis, and (c) the z -axis (wire direction), illustrating anisotropic spatial orientation of surface patches of nanoporous gold.

there are some notable differences. The peak in the ISD of nanoporous gold at $(-1, 1)$ is $\sim 50\%$ higher than for a bicontinuous system coarsening by evaporation/condensation, indicating that there is more interfacial area for curvatures of magnitude S_v^{-1} , and the ISD in the nanoporous gold is compressed toward the $\kappa_2 = -\kappa_1$ line, corresponding to more interfacial area with spherical geometry. Thus a local diffusion mechanism, similar to but different than evaporation/condensation (e.g., surface diffusion), is most probably operational during coarsening of the nanoporous gold.

Detailed analyses of the correlation between structural features and regions curvature on the ISD are shown in Figs. 2(b)–2(d) for a small $600 \times 600 \times 600 \text{ nm}^3$ volume containing a few gold ligaments. Both concave and convex regions are highlighted in Fig. 2(b), corresponding to isolated patches with positive Gaussian curvature. Also visible in a circled region in Fig. 2(b) are remnants of a ligament pinching event which must accompany the increase in size scale during coarsening of any bicontinuous structure. Simulations show that the rate at which these positive Gaussian curvature regions disappear depends on the mass transport mechanism.^{13,14} Their presence in the nanoporous gold may indicate that the mass transport mechanism is not bulk diffusion, which leads to very rapid disappearance of such ligament remains.

Although the ISD shows a nonzero probability for patches with zero Gaussian curvature (i.e., cylindrical patches), these patches do not correspond to cylindrical ligaments in the structure. Rather, as illustrated in Fig. 2(c), these regions with zero Gaussian curvature are scattered throughout the nanoporous gold and are transitions between regions with higher positive and negative mean curvature that also have with negative Gaussian curvature. Another observation is that regions with zero mean curvature form a network throughout the entire sample, as shown in Fig. 2(d). It is thus clear that the nanoporous gold structure is not a minimal surface, a structure with zero mean curvature and nonzero Gaussian curvature at all points.

The morphological anisotropy of the nanoporous gold was characterized by calculating its surface normal distribution (SND), as shown in Fig. 3. SND plots the probability of finding a surface normal pointing in a given direction, as a projection onto a 2D plane taken along one of the coordinates of the 3D reconstruction.¹⁵ Visual inspection of the 3D reconstruction [Fig. 1(b)] gives the qualitative impression that the nanoporous gold is substantially isotropic. The ISD shown in Fig. 3 however clearly shows an anisotropic distribution of surface normals, which does not represent grain effects, since the imaged volume is monocrystalline. There are two possible reasons for the anisotropic SND. First, the

initial dealloying process occurs preferentially along the close-packed $\{111\}$ planes of the alloy,⁵ so that these planes may be preferentially formed along the resulting gold-air interfaces. Second, the subsequent coarsening process may lead to a bias toward surfaces with a lower surface energy γ . In gold at 400 °C, $\gamma\{111\} < \gamma\{100\} < \gamma\{110\}$ and thus preference for $\{111\}$ surfaces is expected.¹⁶ It also has been shown that the $\{111\}$ planes of nanoporous gold can be highly oriented in a specific direction after thermal coarsening.¹⁷ The anisotropy in nanoporous gold surface morphology may affect the properties and functions that are linked to the surface.

In addition to above morphological analysis, we determine the topology of the nanoporous gold sample by calculating its genus, g , which for bicontinuous structures, is related to the number of continuous tunnels or loops in the structure. The genus is determined by computing the surface integral of the Gaussian curvature. In this nanoporous gold sample, the genus per unit volume is $g_v = 48 \mu\text{m}^{-3}$. Thus, in a $1 \mu\text{m}^3$ volume, there are approximately 48 tunnels. Dividing this genus per unit volume with the cube of the specific area provides a dimensionless genus, which for nanoporous gold is 0.147. This gives the number of tunnels on a length scale of S_v^{-1} . By contrast, Schoen's G surface,¹⁸ a minimal surface, has a scaled genus of five, thus a minimal surface does not provide a good description for either the curvatures, as shown above, or for the topology of nanoporous gold. During coarsening of simulated bicontinuous structures,¹⁴ the scaled genus is independent of the mechanism responsible for coarsening (e.g., bulk or evaporation/condensation) and attains a value of ~ 0.13 , reasonably close to the value obtained for the nanoporous gold sample. Thus the nanoporous gold is typologically very similar to the bicontinuous structures created by phase separation.

In summary, we used x-ray nanotomography to image the 3D structure of nanoporous gold fabricated by dealloying and coarsened by annealing. Quantitative analysis of the interface shape and surface normal distributions from 3D reconstructions of the nanotomography data show that the coarsening did not proceed by bulk diffusion, the morphology is anisotropic, and the topology is consistent with bicontinuous structures produced by phase separation. Future time-resolved studies of structural evolution of nanoporous

gold by these methods will provide fundamental scientific insight into nanoporous metals.

We acknowledge Ms. Marie Cox, Mr. Ben Myers, and Dr. Xuexi Zhang (Northwestern University) for assistance with sample preparation. Dr. Wenjun Liu conducted the Laue diffraction at APS beamline 34-ID-E. Alix Deymier (NU) helped with the TXM measurements. Data analysis was assisted by Dr. Dimitris Kammer, Julie Fifth and Larry Aagesen (NU). We thank Dr. Yeukuang Hwu of Academia Sinica for developing the TXM capability at the APS through Partner User Proposal 64 and making it available for general users. Use of the Advanced Photon Source is supported by the U.S. Department of Energy, Office of Science, Office of Basic Energy Sciences, under Contract No. DE-AC02-06CH11357.

¹Y. Ding and M. Chen, MRS Bull. **34**, 8 (2009).

²J. Erlebacher, M. J. Aziz, A. Karma, N. Dimitrov, and K. Sieradzki, *Nature (London)* **410**, 450 (2001).

³R. Li and K. Sieradzki, *Phys. Rev. Lett.* **68**, 1168 (1992).

⁴H. Rösner, S. Parida, D. Kramer, C. A. Volkert, and J. Weissmuller, *Adv. Eng. Mater.* **9**, 535 (2007).

⁵T. Fujita, L.-H. Qian, K. Inoke, J. Erlebacher, and M.-W. Chen, *Appl. Phys. Lett.* **92**, 251902 (2008).

⁶M. D. Uchic, L. Holzer, B. J. Inkson, E. L. Principe, and P. Munroe, MRS Bull. **32**, 408 (2007).

⁷J. Y. Buffiere, P. Cloetens, W. Ludwig, E. Maire, and L. Salvo, MRS Bull. **33**, 611 (2008).

⁸Y. T. Chen, T. N. Lo, Y. S. Chu, J. Yi, C. J. Liu, J. Y. Wang, C. L. Wang, C. W. Chiu, T. E. Hua, Y. Hwu, Q. Shen, G. C. Yin, K. S. Liang, H. M. Lin, J. H. Je, and G. Margaritondo, *Nanotechnology* **19**, 395302 (2008).

⁹J. L. Fife, J. C. Li, D. C. Dunand, and P. W. Voorhees, *J. Mater. Res.* **24**, 117 (2009).

¹⁰Y. S. Chu, J. M. Yi, F. De Carlo, Q. Shen, W. K. Lee, H. J. Wu, C. L. Wang, J. Y. Wang, C. J. Liu, C. H. Wang, S. R. Wu, C. C. Chien, Y. Hwu, A. Tkachuk, W. Yun, M. Feser, K. S. Liang, C. S. Yang, J. H. Je, and G. Margaritondo, *Appl. Phys. Lett.* **92**, 103119 (2008).

¹¹F. Natterer, *The Mathematics of Computerized Tomography* (Wiley, New York, 1986).

¹²J. Alkemper and P. W. Voorhees, *Acta Mater.* **49**, 897 (2001).

¹³Y. Kwon, K. Thornton, and P. W. Voorhees, *Phys. Rev. E* **75**, 021120 (2007).

¹⁴Y. Kwon, K. Thornton, and P. W. Voorhees, *EPL* **86**, 46005 (2009).

¹⁵D. Kammer and P. W. Voorhees, *Acta Mater.* **54**, 1549 (2006).

¹⁶M. Flüeli and J. P. Borel, *J. Cryst. Growth* **91**, 67 (1988).

¹⁷M. Hakamada and M. Mabuchi, *Mater. Lett.* **62**, 483 (2008).

¹⁸W. T. Gózdź and R. Holyst, *Phys. Rev. E* **54**, 5012 (1996).